Energy-Efficient Solutions in Two-user Downlink NOMA Systems Aided by Ambient Backscattering

Hajar El Hassani*, Anne Savard†, E. Veronica Belmega‖*, and Rodrigo C. de Lamare§¶
* ETIS UMR 8051, CY Cergy Paris Université, ENSEA, CNRS, F-95000, Cergy, France
† IMT Nord Europe, Institut Mines Télécom, Centre for Digital Systems, F-59653 Villeneuve d'Ascq, France
‡Univ. Lille, CNRS, Centrale Lille, UPHF, UMR 8520 - IEMN, F-59000 Lille, France
‖ Univ. Gustave Eiffel, CNRS, LIGM, F-77454, Marne-la-Vallée, France
§ CETUC, PUC-Rio, Rio de Janeiro 22451-900, Brazil
¶ Department of Electronics, University of York, York, YO10 5DD, U.K.
Email: hajar.el-hassani@ensea.fr, anne.savard@imt-nord-europe.fr, veronica.belmega@esiee.fr, rcdl500@ohm.york.ac.uk

GLOBECOM 2022 - 2022 IEEE Global Communications Conference | 978-1-6654-3540-6/22/$31.00 ©2022 IEEE | DOI: 10.1109/GLOBECOM48099.2022.10001031

***Abstract*—In this paper, the energy efficiency of a two-user downlink NOMA system aided by several ambient backscatter devices is investigated. We analyze both the tradeoff and the ratio between achievable rates versus power consumption, assuming that the backscatter devices are in fully cooperative mode. In the case of two backscatter devices, we derive a closed-form solution in terms of the optimal reflection coefficients and power allocation policy by exploiting the properties of the energy-efficiency objective and the Pareto boundary of the feasible set. For more than two backscatter devices, the problem becomes difficult and our methodology cannot be extended easily. Nevertheless, we evaluate the performance of NOMA aided by several (up to four) backscatter devices via numerical simulations. Our numerical results show that the energy efficiency of the two-user NOMA system increases with the number of cooperative backscatter devices. Moreover, in the high noise regime, the relative efficiency gain increases with the number of backscatter devices reaching up to 370 % compared to conventional NOMA.**

***Index Terms*—NOMA, energy efficiency maximization, ambient backscatter communications**

I. Introduction

In the past decade, the number of connected devices has increased tremendously, and it is predicted that there will be more than 75 billion connected devices by 2025 [1]. This will lead to the sixth generation (6G) as a key technology for enabling massive internet of things (IoT) connectivity [2], [3]. To ensure an efficient massive connectivity, power-domain non-orthogonal multiple access (NOMA) has emerged [4]. By combining superposition coding and successive interference cancellation (SIC) existing techniques, NOMA can enhance spectrum and energy efficiency by multiplexing several users on the same radio resource (i.e., frequency, time) by cleverly tuning the power allocation policy.

Moreover, since most connected IoT devices are low-powered, new green approaches need to be adopted in 6G networks to efficiently power devices and improve their battery lifetime. Hence, energy harvesting (EH) techniques have been considered a major technology to enhance the energy efficiency in IoT networks. A promising EH techniques in IoT networks is ambient backscatter communication (AmBC) [5]–[8]. Unlike relaying, which is composed of active components requiring a dedicated power source, and unlike reflective intelligent surfaces (RIS), whose main purpose is to enhance the signal quality and assist the transmission of the existing system, an ambient backscattering device (tag) uses the existing radio frequency (RF) signals generated by a source to send information by backscattering a portion of the signal while the remainder is harvested by mismatching the antenna input impedance without requiring any radio frequency (RF) components [6], [7].

Recently, a lot of attention has been dedicated to the study of both power-domain NOMA and ambient backscattering [9]–[13]. In [9], a backscatter cooperation (BC) NOMA scheme was proposed in which the surplus power of the downlink signals received at a user is backscattered to enhance the reception of the user who cannot recover its information. The outage performance and the expected rate were analyzed. The authors in [10] evaluated the performance of a two-user NOMA-backscatter network in terms of bit error rate (BER). In [11], the authors have investigated the ergodic capacity of a downlink NOMA-AmBC network composed of a backscatter device (BD), a base station (BS) and a cellular user. In [12], the authors have proposed a sum-rate optimization framework for a two-user downlink NOMA aided by a backscatter device, under imperfect SIC, in which the reflection coefficient and the transmit power were jointly optimized. Similarly, authors in [13] proposed an iteration algorithm for the optimal joint reflection coefficient and power allocation to enhance the energy efficiency assuming perfect SIC.

In this paper, we study the energy efficiency of a two-user downlink NOMA system aided by several backscatter devices, extending our previous work [14], in which only a single backscatter device was considered. To the best of our knowledge, this is the first work to investigate the energy efficiency of a two-user downlink NOMA system aided by several backscatter devices.

Our main contributions: can be summarized as follows: first, in the case of two backscatter devices, we provide analytical closed-form expressions of the optimal reflection coefficients and the optimal power allocation policy that maximizes the energy efficiency measured as the tradeoff sum rate vs. power consumption; then, we show that the Dinkelbach method maximizing the ratio between sum rate

This work has been supported by the ELIOT ANR-18-CE40-0030 and FAPESP 2018/12579-7 project and IRCICA, CNRS USR 3380, Lille, France.

and power consumption is reduced to a line search as a result of our closed-form solution; at last, via numerical results we analyze the energy efficiency of our NOMA system aided by several (up to four) backscatter devices. Compared with conventional NOMA (without backscattering), we show that the energy-efficiency gain increases with the number of backscatter devices, reaching up to 370% (for four backscatter devices) in the high noise regime.

Compared to our previous work in [14], the novel contributions are two-fold. First, when moving from one to two backscatter devices, although the methodology is similar, finding the closed-form expressions of the optimal reflection coefficients is not trivial. Indeed, the additional control variable (i.e., the second backcatter device's reflection coefficient) significantly changes the structure of the feasible set and of its Pareto boundary. Moreover, we conjecture that for an arbitrary number of backscatter devices, such an analytical solution is very difficult if not impossible to find. Second, via numerical simulations, we investigate the energy efficiency in the cases of three and four backscatter devices, which allows us to draw conclusions in the general case.

II. System model

For simplicity and clarity of presentation, we focus on the case of two backscatter devices case, unless specified otherwise.[1] The downlink NOMA system under study is composed of one RF source (e.g., BS, access point, etc.) and two users $U_i, i \in \{1,2\}$, where the transmission is assisted by two backscatter devices $BD_i, i \in \{1,2\}$, as depicted in Fig. 1. Both users are served in a non-orthogonal manner by the source: the messages $X_i \sim \mathcal{N}(0,1)$ intended for each of the users U_i are superposed to form the signal $X = \sqrt{P_1}X_1 + \sqrt{P_2}X_2$ that is broadcast to both users, where P_i denotes the power allocated to user X_i, $i \in \{1,2\}$. Both backscatter devices are assumed to be fully cooperative and always reflect the incoming signals [5], [15].

We denote by h_i, g_i and g_{ij} the channel gains between the source and user U_i, between the source and backscatter device BD_i and between backscatter device BD_i and user U_j, respectively. We also denote by $Z_i \sim \mathcal{N}(0,\sigma_i^2)$ the additive white Gaussian noise at each user U_i which is independent from X_i. At last, we assume that the decoding order at the users' side is decided based on the ordering of the channel gains between the source and the users. Without loss of generality, we assume that $\frac{|h_1|^2}{\sigma_1^2} \geq \frac{|h_2|^2}{\sigma_2^2}$, such that user U_1 carries out SIC and user U_2 suffers the interfering message intended for user U_1.

The received signal at user U_i writes as

$$Y_i = \left(h_i + \sqrt{\rho_1}g_1 g_{1i} + \sqrt{\rho_2}g_2 g_{2i}\right) X + Z_i, \ \forall i \in \{1,2\} \quad (1)$$

where ρ_1 and ρ_2 denote the reflection coefficients of the backscatter devices.

[1] All the derivations in this section carry over to the case of an arbitrary number of backscatter devices, which will be investigated via numerical results in Sec. IV.

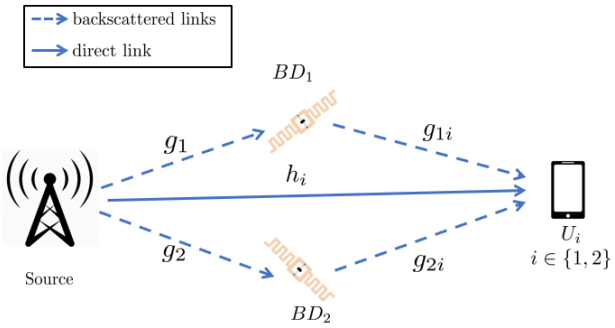

Fig. 1. Illustration of two-backscatter two-user downlink NOMA-AmBC system

A. Achievable rate region

User U_1 performs SIC, where he firstly decodes the message X_2 destined for user U_2 while treating his own message X_1 an interference. To ensure a successful decoding of X_2 it is required that

$$R_2 \leq R_{2\to 1} \triangleq C\left(\frac{P_2\Gamma_1(\rho_1,\rho_2)}{P_1\Gamma_1(\rho_1,\rho_2)+1}\right), \quad (2)$$

with $C(x) \triangleq 1/2\log_2(1+x)$ denoting the Shannon capacity and the notations below

$$\Gamma_1(\rho_1,\rho_2) = (G_1 + \sqrt{\rho_1}G_{11} + \sqrt{\rho_2}G_{21})^2;$$
$$G_1 = \frac{h_1}{\sigma_1}; G_{11} = \frac{g_1 g_{11}}{\sigma_1}; G_{21} = \frac{g_2 g_{21}}{\sigma_1}.$$

After successfully decoding X_2, user U_1 deletes the message X_2 from its observation and decodes its own message X_1. In this case to successfully decode the message X_1 the achievable rate of user 1 is

$$R_1 = C(P_1\Gamma_1(\rho_1,\rho_2)). \quad (3)$$

At user U_2, the message intended for user U_1 is treated as an additional noise, hence perfect recovering of the message X_2 requires that

$$R_2 \leq R_{2\to 2} \triangleq C\left(\frac{P_2\Gamma_2(\rho_1,\rho_2)}{P_1\Gamma_1(\rho_1,\rho_2)+1}\right), \quad (4)$$

with the notations

$$\Gamma_2(\rho_1,\rho_2) = (G_2 + \sqrt{\rho_1}G_{12} + \sqrt{\rho_2}G_{22})^2;$$
$$G_2 = \frac{h_2}{\sigma_2}; G_{12} = \frac{g_1 g_{12}}{\sigma_2}; G_{22} = \frac{g_2 g_{22}}{\sigma_2}.$$

To sum up, the achievable data rates are provided in the following proposition.

Proposition 1. *The achievable rate region of two-user downlink NOMA system assisted by two backscatter devices writes as*

$$R_1 = C(P_1\Gamma_1(\rho_1,\rho_2)) \text{ and } R_2 = \min\{R_{2\to 1}, R_{2\to 2}\},$$

where $R_{2\to i}$ defined above represent the achievable rate ensuring successful decoding of the message X_2 at user i.

B. Energy efficiency maximization

We focus on optimizing the tradeoff between achievable sum rate vs. total power consumption [16], where the total power budget of the source is limited by $\overline{P}$ and each user $U_i, i \in \{1,2\}$ has to meet a minimum rate level $\overline{R_i}$. Furthermore, to ensure a successful SIC operation, the following condition has to be met: $R_{2\to 2} \le R_{2\to 1}$ [13].

The resulting optimization problem can be written as follows

$$(\mathbf{EE1}) \max_{\rho_1,\rho_2,P_1,P_2} \; C(P_1\Gamma_1(\rho_1,\rho_2))+C\left(\frac{P_2\Gamma_2(\rho_1,\rho_2)}{1+P_1\Gamma_2(\rho_1,\rho_2)}\right) - \alpha(P_1+P_2+P_c)$$

$$\begin{aligned} \text{s.t.} \quad & (C1) \quad 0 \le \rho_1,\rho_2 \le 1 \\ & (C2) \quad \Gamma_1(\rho_1,\rho_2) \ge \Gamma_2(\rho_1,\rho_2), \\ & (C3) \quad P_1 \ge \frac{2^{2\overline{R_1}}-1}{\Gamma_1(\rho_2,\rho_2)}, \\ & (C4) \quad P_2 \ge \left(2^{2\overline{R_2}}-1\right)\left(P_1+\frac{1}{\Gamma_2(\rho_1,\rho_2)}\right), \\ & (C5) \quad P_1+P_2 \le \overline{P}, \end{aligned}$$

where α is the parameter that trades-off between the sum rate and the total power consumption, the constraint $(C1)$ is the range of the reflection coefficients, $(C2)$ derives from the successful SIC condition $R_{2\to 2} \le R_{2\to 1}$; $(C3)$ and $(C4)$ derive from the minimum achievable rate constraints $C(P_1\Gamma_1(\rho_1,\rho_2)) \ge \overline{R}_1$ and $C\left(\frac{P_2\Gamma_2(\rho_1,\rho_2)}{1+P_1\Gamma_2(\rho_1,\rho_2)}\right) \ge \overline{R}_2$ of user U_1 and U_2 respectively; $C(5)$ is the power budget constraint where $\overline{P}$ is the maximum power at the source and P_c denotes the overall circuit power consumption.

III. Optimal closed-form solution

The problem $(\mathbf{EE1})$ is not convex due to the joint optimization of the reflection coefficients ρ_1 and ρ_2 and the allocated powers P_1 and P_2. Nevertheless, we can exploit a similar approach as in [14] and solve the problem by decoupling it into two sub-problems without loss of optimality such that we first optimize (ρ_1,ρ_2) for an arbitrary power allocation and then optimize (P_1,P_2) with the obtained optimal reflection coefficients ρ_1^* and ρ_2^*.

A. Optimal reflection coefficients

We fix an arbitrary power allocation policy (P_1,P_2) and solve $(\mathbf{EE1})$ w.r.t. the reflection coefficients only. Note that the objective function in $(\mathbf{EE1})$ is increasing w.r.t ρ_1 and ρ_2 unilaterally, which means that the optimal values ρ_1^* and ρ_2^* lie on the Pareto boundary of the feasible set.

Theorem 1. *For any feasible power allocation policy (P_1,P_2), the optimal values of the reflection coefficients ρ_1^* and ρ_2^* of $(\mathbf{EE1})$ can be found in closed form as follows. Let*

$$\overline{\rho_1} = \left(\frac{G_1-G_2}{G_{12}-G_{11}}\right)^2, \widetilde{\rho_1} = \left(\frac{G_1-G_2-(G_{22}-G_{21})}{G_{12}-G_{11}}\right)^2$$

$$\overline{\rho_2} = \left(\frac{G_1-G_2}{G_{22}-G_{21}}\right)^2, \widetilde{\rho_2} = \left(\frac{G_1-G_2-(G_{12}-G_{11})}{G_{22}-G_{21}}\right)^2.$$

[H1] If $(G_{12}-G_{11}) \le 0$ ***and*** $(G_{22}-G_{21}) \le 0$, *then* $\rho_1^*=\rho_2^*=1$.
[H2] If $(G_{12}-G_{11}) \le 0$ ***and*** $(G_{22}-G_{21}) > 0$, *then* $\rho_1^*=1; \rho_2^*=\min\{1,\widetilde{\rho_2}\}$.
[H3] If $(G_{12}-G_{11}) > 0$ ***and*** $(G_{22}-G_{21}) \le 0$, *then* $\rho_1^*=\min\{1,\widetilde{\rho_1}\}; \rho_2^*=1$.
[H4] If $(G_{12}-G_{11})>0$ ***and*** $(G_{22}-G_{21})>0$, *then*
i) If $G_{22}G_{11}-G_{12}G_{21} \ge 0$*:* $\rho_1^*=\min\{1,\overline{\rho_1}\}; \rho_2^*=\min\{1,\max\{0,\widetilde{\rho_2}\}\}$;
ii) If $G_{22}G_{11}-G_{12}G_{21}<0$*:* $\rho_1^*=\min\{1,\max\{0,\widetilde{\rho_1}\}\}; \rho_2^*=\min\{1,\overline{\rho_2}\}$.

The detailed proof is provided in the Appendix.

B. Optimal power allocation

Now, since the expressions of the optimal reflection coefficients above are independent from the power allocation policy, and given that the larger the reflection coefficients are, the smaller the minimum power required to fulfill each QoS constraint in $(C3)$ and $(C4)$ is. Thus, choosing (ρ_1^*,ρ_2^*) as in Theorem 1 does not incur an optimality loss.

Moreover, for (ρ_1^*,ρ_2^*) in Theorem 1, we have the channel order $\Gamma_1(\rho_1^*,\rho_2^*) \ge \Gamma_2(\rho_1^*,\rho_2^*)$, and hence our optimization problem reduces to

$$(\mathbf{EE2}) \max_{P_1,P_2} \; C(P_1\Gamma_1(\rho_1^*,\rho_2^*))+C\left(\frac{P_2\Gamma_2(\rho_1^*,\rho_2^*)}{1+P_1\Gamma_2(\rho_1^*,\rho_2^*)}\right) - \alpha(P_1+P_2+P_c)$$

$$\begin{aligned} \text{s.t.} \quad & (C1') \quad P_1 \ge \frac{2^{2\overline{R_1}}-1}{\Gamma_1(\rho_1^*,\rho_2^*)} \\ & (C2') \quad P_2 \ge \left(2^{2\overline{R_2}}-1\right)\left(P_1+\frac{1}{\Gamma_2(\rho_1^*,\rho_2^*)}\right) \\ & (C3') \quad P_1+P_2 \le \overline{P}, \end{aligned} \tag{5}$$

which is a convex problem and can be solved in closed form following our previous work in [17]. For the sake of completeness we provide below the optimal power allocation policy (P_1^*,P_2^*).

Proposition 2. *The sufficient and necessary condition on the optimization problem (5) feasibility is given by*

$$\overline{P} \ge P_{\min} = \frac{2^{2\overline{R_2}}-1}{\Gamma_2(\rho_1^*,\rho_2^*)} + \frac{(2^{2\overline{R_1}}-1)2^{2\overline{R_2}}}{\Gamma_1(\rho_1^*,\rho_2^*)}, \tag{6}$$

and the optimal power allocation of both users is provided as

$$P_1^* = \min\left\{\max\left\{\frac{2^{2\overline{R_1}}-1}{\Gamma_1(\rho_1^*,\rho_2^*)}, \widetilde{P_1}\right\}, \frac{\overline{P}-\frac{2^{2\overline{R_2}}-1}{\Gamma_2(\rho_1^*,\rho_2^*)}}{2^{2\overline{R_2}}}\right\} \tag{7}$$

$$P_2^* = \left(2^{2\overline{R_2}}-1\right)\left(P_1^*+\frac{1}{\Gamma_2(\rho_1^*,\rho_2^*)}\right), \tag{8}$$

with

$$\widetilde{P_1} = \frac{1}{(2\ln 2)\alpha}\frac{1}{2^{2\overline{R_2}}} - \frac{1}{\Gamma_1(\rho_1^*,\rho_2^*)}. \tag{9}$$

C. Multi-user multi-backscatter device case

In the case of $K > 2$ users and two backscater devices, since the successful SIC constraint becomes $\Gamma_{(k-1)}(\rho_1, \rho_2) \geq \Gamma_k(\rho_1, \rho_2), \forall k \in \{1, \ldots, K\}$, the optimization problem (**EE1**) becomes hard to solve w.r.t the reflection coefficients pair (ρ_1, ρ_2). In this case, according to Theorem 1, six cases need to be discussed for each pair $\Gamma_{k-1}(\rho_1, \rho_2) \geq \Gamma_k(\rho_1, \rho_2)$. Since the obtained ρ_1^* and ρ_2^* are coupled, one has to find the feasibility region defined by the set of all $(K-1)$ successful SIC constraints, which is obtained through a nested six cases loop. Thus, generalizing our solution to the multi-user case is not trivial.

In the case of multi-backscatter devices, the graphical method by which we have obtained Pareto boundary of the feasible reflection coefficients is very limited, since no physical image of the feasible set is possible beyond two helping devices. The constraint $(C2)$ becomes a multi-variable inequality, and, hence it is necessary to exploit a more general (algorithmic) method to solve the problem. Moreover, the number of cases discussed in Theorem (1) will grow exponentially with the number of backscatter devices, which further complicates the extension of our closed-form solution.

D. Sum rate vs. power consumption ratio

A different popular metric named the global energy efficiency (GEE) [16] is defined as the ratio between the achievable sum rate and the total power consumption:

$$GEE(\rho_1, \rho_2, P_1, P_2) = \frac{C(P_1\Gamma_1(\rho_1, \rho_2)) + C\left(\frac{P_2\Gamma_2(\rho_1,\rho_2)}{1+P_1\Gamma_2(\rho_1,\rho_2)}\right)}{P_1 + P_2 + P_c}. \tag{10}$$

We can show that GEE can be maximized using Dinkelbach's method [16] and that our closed-form solution reduces the inner loop of the algorithm to a simple line search, similarly to [14]. Let $R_{\text{sum}}^* = C(P_1^*\Gamma_1(\rho_1^*, \rho_2^*)) + C\left(\frac{P_2^*\Gamma_2(\rho_1^*,\rho_2^*)}{1+P_1^*\Gamma_2(\rho_1^*,\rho_2^*)}\right)$ and $P_{\text{tot}}^* = P_1^* + P_2^* + P_c$, the Dinkelbach's algorithm is given as follows

Algorithm 1 GEE maximization with Dinkelbach

$\epsilon > 0$, $\alpha = 0$
Compute (ρ_1^*, ρ_2^*) via Theorem (1)
while $F(\alpha) \leq \epsilon$ **do**
  Compute P_1^*, P_2^* via eq. (7) and (8) resp.
  Update $F(\alpha) = R_{\text{sum}}^* - \alpha P_{\text{tot}}^*$
  Update $\alpha \leftarrow GEE(\rho_1^*, \rho_2^*, P_1^*, P_2^*)$
end while

IV. Numerical simulations

In this section, we present simulations results for a two-user downlink NOMA system assisted by two ambient backscatter devices where we evaluate the GEE using algorithm (1). The channels are assumed to follow a path loss model: $d^{-\eta}$, where d is distance between different nodes and η is the path loss exponent. The results are averaged over 10^3 independent random draws of the nodes positions. The two users are randomly located within a cell of radius 15 m. The maximum distance between the two backscatter devices and the base station is 3 m. The pathloss exponent is $\eta = 2.5$. The system parameters are $\overline{P} = 40$ dBm, $P_c = 30$ dBm, $\sigma_i^2 = \sigma^2 = -20$ dBm and $\overline{R_i} = \overline{R}, i \in \{1, 2\}$.

We compare our proposed solution with three benchmarks: OMA with two backscatter devices, NOMA with one backscatter device as well as conventional NOMA (without backscattering). More importantly, we also analyze here the more general case of three and four backscatter-aided NOMA schemes, whose solutions are obtained via exhaustive search, and investigate the energy efficiency as a function of the number of cooperative backscatter devices.

Fig. 2 depicts the GEE as a function of $\overline{R}$. We see that NOMA with two backscatter devices outperforms NOMA with a single backscatter device, which outperforms OMA with two backscatter devices. For larger minimum QoS levels, the GEE decreases since more power is consumed to meet the users' QoS constraints. At last, we see that GEE increases with the number of cooperative backscatter devices.

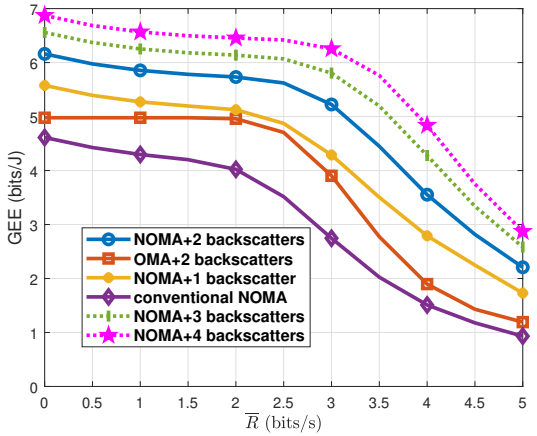

Fig. 2. Energy efficiency (GEE) as a function of $\overline{R}$. Two backscatter-aided NOMA outperforms the benchmark schemes. The gain increases with the number of backscatter devices.

Fig. 3 depicts the GEE as a function of $\overline{P}$. We see that our proposed scheme outperforms all other benchmarks irrespective from $\overline{P}$. Furthermore, GEE increases with the number of cooperative backscatter devices and with $\overline{P}$ until it reaches a flat level, beyond which increasing the power has no longer effect on the GEE.

At last, in Fig. 4 we plot the relative gain of the different schemes compared to conventional NOMA, defined as $\left(GEE^{\text{scheme}} - GEE^{\text{NOMA}}\right)/GEE^{\text{NOMA}}$, as a function of the noise variance σ^2. We see that the relative gain increases with σ^2 to reach up to 220%, 170% and 110% for NOMA with two backscatters, OMA with two backscatters and NOMA with a single backscatter, respectively. Moreover, the more the number of cooperative backscatter devices, the larger the gain performance achieved by NOMA: reaching up to 370% for four backscatter devices in the high noise regime.

The incremental gap between the successive curves for backscatter-aided NOMA in Fig. 3, Fig. 2, and Fig. 4 seems to be closing when increasing the number of backscatter devices, leading us to the open question of finding the number of optimal backscatter devices.

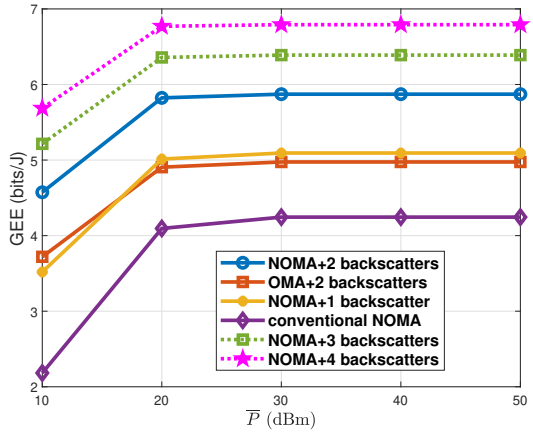

Fig. 3. Energy efficiency as a function of $\overline{P}$ where $\overline{R} = 1$ bit/s. Two backscatters-aided NOMA always outperforms other benchmark schemes and the energy efficiency increases with the number of backscatter devices regardless of $\overline{P}$.

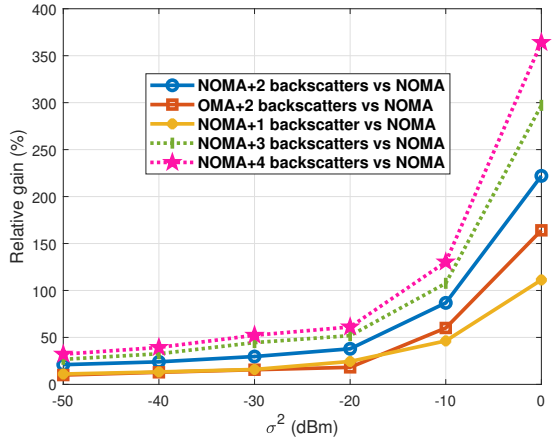

Fig. 4. Relative gain of backscatter-aided NOMA compared to conventional NOMA as a function of σ^2 for one, two, three and four backscatter devices. In the high noise regime, the larger the number of backscatter devices, the larger the gain compared to conventional NOMA.

V. Conclusion

In this paper, we investigated the energy-efficiency maximization of a two-user downlink NOMA system assisted by several ambient backscatter devices. For the case of two backscatter devices, we provided the optimal solution, i.e., optimal reflection coefficients and power allocation policy, in analytical closed-form. Our numerical results show that NOMA with two ambient backscatter devices outperforms the benchmark schemes. Moreover, our simulations show that the energy efficiency increases with the number of cooperative backscatter devices. In the high noise regime, the relative gain compared to conventional NOMA increases with the number of backscatter devices, reaching up to 370 %. However, the incremental gap seems to be closing, leading to the question of finding the optimal number of such helping devices, which is left open for future investigation.

VI. Appendix: Proof of the Main Theorem

Since the objective function of (**EE1**) is increasing w.r.t ρ_1 for fixed P_1, P_2 and ρ_2; and, is also increasing w.r.t. ρ_2 for fixed P_1, P_2 and ρ_1; the optimal reflection coefficients lie on the Pareto boundary (i.e., all feasible points such that none of their coordinates can be increased while remaining feasible) of the feasible set defined by the constraints $(C1) - (C2)$. Note that after some mathematical derivations, the constraint $(C2)$ can be rewritten as $\sqrt{\rho_1}(G_{12} - G_{11}) + \sqrt{\rho_2}(G_{22} - G_{21}) \leq G_1 - G_2$.

We now provide the optimal values of (ρ_1, ρ_2) by analyzing geometrically the feasible set and its Pareto optimal boundary in the four possible cases given in Theorem 1.

A. Case [H1]: $(G_{12} - G_{11}) \leq 0$ and $(G_{22} - G_{21}) \leq 0$

In this case, since $(G_1 - G_2) \geq 0$ by assumption, the constraints are always fulfilled for all values of $\rho_1, \rho_2 \in [0, 1]$. Hence, the optimal solution is unique $\rho_1^* = \rho_2^* = 1$.

B. Case [H2]: $(G_{12} - G_{11}) \leq 0$ and $(G_{22} - G_{21}) > 0$

Under [H2], one can show that $\overline{\rho_1} < 0$; $\overline{\rho_2} \geq 0$ and $\widetilde{\rho_2} > \overline{\rho_2}$. Several cases can arise depending on the value of $\overline{\rho_2}$ as depicted in Fig. 5.

[H21] If $\overline{\rho_2} > 1$, which leads to $\widetilde{\rho_1} < 0$ and $\widetilde{\rho_2} > 1$, the optimal solution is unique: $\rho_1^* = \rho_2^* = 1$.

Otherwise $\overline{\rho_2} \leq 1$ leads to $\widetilde{\rho_1} \geq 0$ and $\widetilde{\rho_2} > \overline{\rho_2} \geq 0$. Two sub-cases arise: either **[H221]** if $\widetilde{\rho_2} > 1$, then $\rho_1^* = \rho_2^* = 1$; or **[H222]** if $\widetilde{\rho_2} \leq 1$, then the Pareto optimal boundary also reduces to a unique point $\rho_1^* = 1, \rho_2^* = \widetilde{\rho_2}$.

Hence to summarize, the optimal values of the reflection coefficients are given as $\rho_1^* = 1; \rho_2^* = \min\{1, \widetilde{\rho_2}\}$.

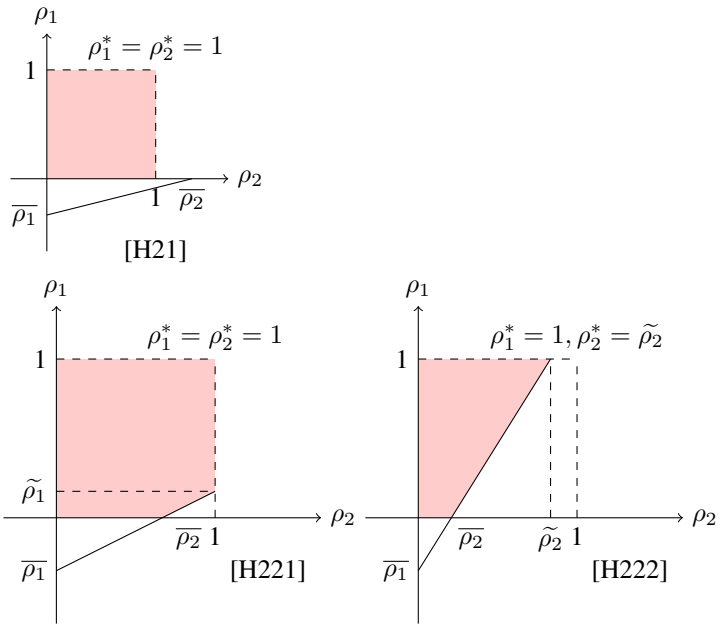

Fig. 5. The three cases that can arise under [H2]: the feasible set is depicted in red. The Pareto boundary reduces to a unique solution.

C. Case [H3]: $(G_{12} - G_{11}) > 0$ and $(G_{22} - G_{21}) \leq 0$

This case is similar to the previous case [H2], hence the detailed proof is omitted.

D. Case [H4]: $(G_{12} - G_{11}) > 0$ and $(G_{22} - G_{21}) > 0$

We can prove the following:
$\overline{\rho_i} \geq 0$ and $\widetilde{\rho}_i \leq \overline{\rho_i}$, $\forall i \in \{1, 2\}$;
If $\overline{\rho_i} > 1$, then $\widetilde{\rho}_j > 0$, $\forall i, j \in \{1, 2\}$ s.t. $j \neq i$;
If $\overline{\rho_i} < 1$, then $\widetilde{\rho}_j < 0$, $\forall i, j \in \{1, 2\}$ s.t. $j \neq i$;
If $\widetilde{\rho}_i > 1$, then $\widetilde{\rho}_j > 1$, $\forall i, j \in \{1, 2\}$ s.t. $j \neq i$;
If $\widetilde{\rho}_i < 1$, then $\widetilde{\rho}_j < 1$, $\forall i, j \in \{1, 2\}$ s.t. $j \neq i$.

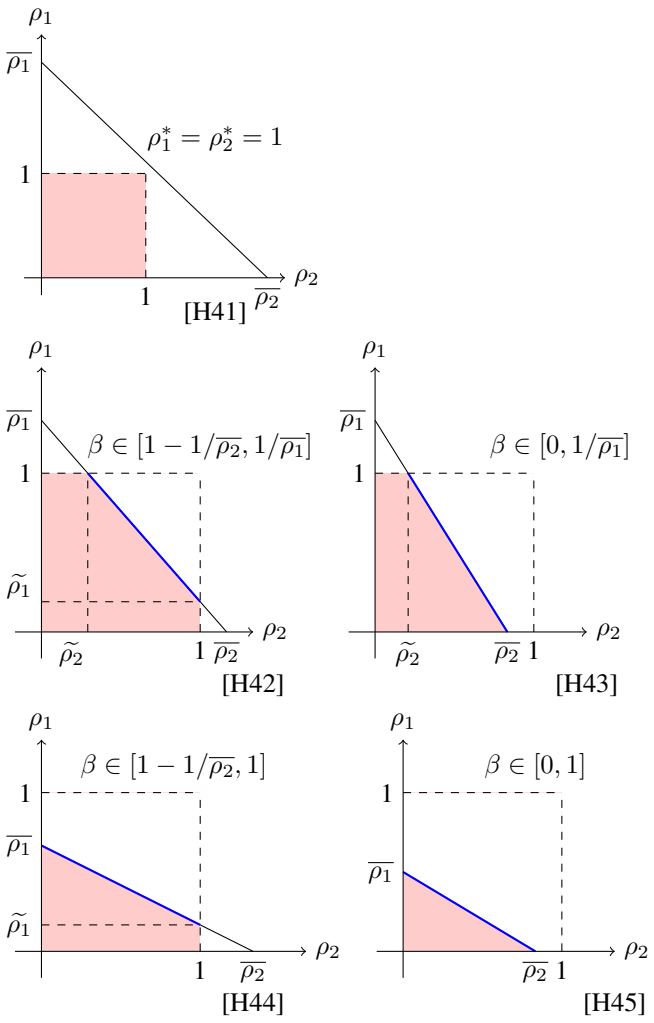

Fig. 6. The five cases that can arise under [H4]: the feasible set is depicted in red. The Pareto boundary in cases [H42]-[H44] is the blue segment given by $\rho_1 = \beta\overline{\rho_1}; \rho_2 = (1 - \beta)\overline{\rho_2}$.

The optimal solution lies on the Pareto boundary of the feasible set depicted in red in Fig. 6. Note that except for the sub-case [H41], the Pareto boundary of the feasible set is not unique but a continuous segment (in blue) of the line between $\overline{\rho_1}$ and $\overline{\rho_2}$. This set can be characterized in a parametric manner as $\rho_1 = \beta\overline{\rho_1}$, $\rho_2 = (1-\beta)\overline{\rho_2}$, where β ranges over the interval specified in each subcases of Fig. 6. Note that except for subcase [H41], $\Gamma_1(\rho_1, \rho_2) = \Gamma_2(\rho_1, \rho_2)$.

In [H41], both $\overline{\rho_i}$ and $\widetilde{\rho}_i$, $i \in \{1, 2\}$, are larger than 1, hence the optimal solution is $\rho_1^* = \rho_2^* = 1$.

In the other four cases, we need to find the reflection coefficients on the Pareto boundary: $\rho_1 = \beta\overline{\rho_1}$, $\rho_2 = (1-\beta)\overline{\rho_2}$, which maximize the objective function. Hence, the problem is reduced to a single variable optimization over β, whose objective is

$$f(\beta) = \log_2 \left(1 + (P_1 + P_2)(G_2 + \beta\overline{\rho_1}G_{12} + (1 - \beta)\overline{\rho_2}G_{22})\right)$$

of derivative

$$\begin{aligned}\frac{\partial f(\beta)}{\partial \beta} &= \frac{(P_1 + P_2)(G_{12}\overline{\rho_1} - G_{22}\overline{\rho_2})}{\ln 2(1 + (P_1 + P_2)\Gamma_2(\beta))} \\ &\propto (G_{12}\overline{\rho_1} - G_{22}\overline{\rho_2}) \\ &\propto \frac{(G_1 - G_2)(G_{22}G_{11} - G_{12}G_{21})}{(G_{12} - G_{11})(G_{22} - G_{21})}.\end{aligned}$$

Hence, the objective function is either decreasing or increasing w.r.t. β depending on the sign of $(G_{22}G_{11} - G_{12}G_{21})$.

- If $(G_{22}G_{11} - G_{12}G_{21}) \geq 0$, the objective function is increasing in β, hence its optimal value is the upper-bound of its feasible interval, specified in each sub-case.
- If $(G_{22}G_{11} - G_{12}G_{21}) < 0$, the objective function is decreasing in β, hence its optimal value is the lower-bound of its feasible interval, specified in each sub-case.

REFERENCES

[1] L. Horwitz, "The future of IoT miniguide: The burgeoning IoT market continues," *CISCO, San Jose, CA, USA, Tech. Rep*, 2019.
[2] S. Verma, S. Kaur, M. A. Khan, and P. S. Sehdev, "Toward green communication in 6G-Enabled Massive Internet of Things," *IEEE Internet Things J.*, vol. 8, no. 7, pp. 5408–5415, 2021.
[3] M. Giordani, M. Polese, M. Mezzavilla, S. Rangan, and M. Zorzi, "Toward 6G networks: Use cases and technologies," *IEEE Commun. Mag.*, vol. 58, no. 3, pp. 55–61, 2020.
[4] N. H. Mahmood, H. Alves, O. A. López, M. Shehab, D. P. M. Osorio, and M. Latva-Aho, "Six key features of machine type communication in 6G," in *IEEE 2nd 6G Wireless Summit (6G SUMMIT)*, 2020, pp. 1–5.
[5] V. Liu, A. Parks, V. Talla, S. Gollakota, D. Wetherall, and J. R. Smith, "Ambient backscatter: Wireless communication out of thin air," *ACM SIGCOMM Computer Communication Review*, vol. 43, no. 4, pp. 39–50, 2013.
[6] G. Wang, F. Gao, R. Fan, and C. Tellambura, "Ambient backscatter communication systems: Detection and performance analysis," *IEEE Trans. Commun.*, vol. 64, no. 11, pp. 4836–4846, 2016.
[7] C. Boyer and S. Roy, "Backscatter communication and RFID: Coding, energy, and MIMO analysis," *IEEE Trans. Commun.*, vol. 62, no. 3, pp. 770–785, 2014.
[8] F. Jameel and S. A. Hassan, *Wireless-Powered Backscatter Communications for Internet of Things*. Springer, 2020.
[9] W. Chen, H. Ding, S. Wang, D. B. da Costa, F. Gong, and P. H. J. Nardelli, "Backscatter cooperation in NOMA communications systems," *IEEE Trans. Wireless Commun.*, vol. 20, no. 6, pp. 3458–3474, 2021.
[10] A. W. Nazar, S. A. Hassan, and H. Jung, "BER analysis of a NOMA enhanced backscatter communication system," in *IEEE GLOBECOM*, 2020, pp. 1–6.
[11] W. Chen, H. Ding, S. Wang, D. B. da Costa, F. Gong, and P. H. J. Nardelli, "Ambient backscatter communications over NOMA downlink channels," *China Commun.*, vol. 17, no. 6, pp. 80–100, 2020.
[12] W. U. Khan, X. Li, M. Zeng, and O. A. Dobre, "Backscatter-enabled NOMA for future 6G systems: A new optimization framework under imperfect SIC," *IEEE Commun. Lett.*, 2021.
[13] Y. Xu, Z. Qin, G. Gui, H. Gacanin, H. Sari, and F. Adachi, "Energy efficiency maximization in NOMA enabled backscatter communications with QoS guarantee," *IEEE Wireless Commun. Lett.*, 2020.
[14] H. El Hassani, A. Savard, E. V. Belmega, and R. C. De Lamare, "Energy-efficient cooperative backscattering closed-form solution for NOMA," in *IEEE GLOBECOM*, 2021, pp. 1–6.
[15] S. Zhou, W. Xu, K. Wang, C. Pan, M.-S. Alouini, and A. Nallanathan, "Ergodic rate analysis of cooperative ambient backscatter communication," *IEEE Wireless Commun. Lett.*, vol. 8, no. 6, pp. 1679–1682, 2019.
[16] A. Zappone and E. Jorswieck, "Energy efficiency in wireless networks via fractional programming theory," *Foundations and Trends in Communications and Information Theory*, vol. 11, no. 3-4, pp. 185–396, 2015.
[17] H. El Hassani, A. Savard, and E. V. Belmega, "A closed-form solution for energy-efficiency optimization in multi-user downlink NOMA," in *IEEE PIMRC*, 2020, pp. 1–5.